REVIEW ARTICLE

Cardiac Amyloidosis: Current Diagnostic Strategies Using Multimodality Imaging

Kenji Fukushima, MD, PhD[1), 2)], Shintaro Nakano, MD, PhD[2)] and Ichiro Matsunari, MD, PhD[3)]

Received: July 10, 2020/Revised manuscript received: July 27, 2020/Accepted: July 27, 2020

Abstract

Amyloidosis is a systemic disorder in which abnormal amyloid proteins deposit in body organs, leading to organ dysfunction and death. Cardiac amyloid deposition, causing a sort of restrictive cardiomyopathy and associated with increased risk of mortality. Most cases of cardiac amyloidosis are of either light chain or transthyretin type. Early and accurate diagnosis of cardiac amyloidosis may improve outcomes. However, diagnosis requires systematic approach including electrocardiography and biomarkers when encountered suspicious candidate. Diagnosis by multimodality noninvasive imaging have been substantially studied and established for differentiation from subtypes. Recent advance in the treatment of amyloidosis offers therapeutic monitoring and prognosis.

Keywords: Cardiac amyloidosis, Cardiac imaging, Cardiomyopathy, Multimodality, Nuclear cardiology
Ann Nucl Cardiol 2020; 6 (1): 67–73

Amyloidosis is systemic disorders due to irreversible deposition of abnormally conformed protein in multiple organs including myocardium. The disease is classified by the misfolded precursor protein and display significant heterogeneity in clinical course, prognosis and treatment considerations that depend upon the involved organs and the type of protein. Cardiac involvement causes amyloid fibrils deposition in myocardium leads to extracellular accumulation of misfolded protein fragments (1). Thus, cardiac amyloidosis (CA) manifest a sort of restrictive cardiomyopathy with left ventricular hypertrophy characterized by rapid progressive heart failure, conduction abnormalities, fatal arrhythmias, and is associated with high mortality (2). In clinical practice, although the physicians encounter various types of CA including subtypes of hereditary and acquired, majority of the cases are caused by light chain (AL) or transthyretin amyloidosis (ATTR), with the latter including two subtypes: wild-type transthyretin deposition, and familial ATTR. As a field of clinical and scientific investigation using noninvasive imaging, those major 2 CA has been a primal target to elucidate. Early and accurate differential diagnosis is of great significance in offering more therapeutic option (3).

In the following review, we addressed the clinical value for noninvasive diagnostic tools and future potential.

Echocardiography

Table 1 shows the noninvasive tools for CA currently available in clinical or preclinical practice. Echocardiography (Echo) is an easy to access at bedside, common noninvasive technique without radiation exposure. In the clinical experience and work up for CA, diagnosis by Echo has been established to identify the patients who suspect of CA showing likely to have the disease and prompting further workup (4). Unlike nuclear technique, Echo can demonstrate multiparametric analysis in reginal wall and global cardiac performance simultaneously. A widely recognized finding is myocardial granular sparkling appearance, which is attributed to the increased echogenicity due to the deposition of amyloid fibrils (4). The left panel of figure 1 shows a patient with CA who presented low voltage in rim leads and typical granular sparking which represents high echoic signal in septal wall implying deposition of amyloid fibrils (yellow arrows).

doi: 10.17996/anc.20-00130

1) Department of Nuclear Medicine, Heart Center, Saitama Medical University International Medical Center, Saitama, Japan
2) Department of Cardiology, Heart Center, Saitama Medical University International Medical Center, Saitama, Japan
3) Department of Nuclear Medicine, Saitama Medical University, Saitama, Japan

Table 1 Noninvasive modality for cardiac amyloidosis

Modality	Technique/Feature	Contrast agent/Tracers	Target subtypes	Advantage or Potential/Limitation
Echocardiography	B or M-mode E'/A' Strain	None	ATTR, AL	Acoustic penetration
CMR	Cine Tagging Feature tracking		ATTR, AL	CKD, Device implantation
	LGE T1mapping	Gadolinium		
SPECT				
^{99m}Tc PYP ^{99m}Tc DPD ^{99m}Tc HMDP ^{99m}Tc MDP	Planar, Heart/Contralateral lung ratio	Bone avid	ATTR	Bone uptake
^{99m}Tc aprotinin	Planar			Liver uptake
PET				
^{11}C-PiB				Cyclotron demand
^{18}F-Florbetapir ^{18}F-Flutemetamol ^{18}F-Florbetaben	PETCT	Amyloid biding	ATTR, AL	Delivery
^{18}F-NaF		Bone avid	ATTR	

Additionally, abnormal thickening of atrial wall and valvular leaf are also found in specific types of CA, such as ATTR amyloidosis (4). Accumulated data suggest the importance of employing more multiparametric imaging over conventional B or M-mode technique such as Tissue Doppler Imaging (TDI), and speckle tracking. However, TDI has many technical limitations based on doppler effect (5). Speckle tracking technique has been more extensively investigated to evaluate longitudinal, radial and circumferential deformations in LV. Several investigators reported the utility of the global and regional strain parameters to differentiate CA from HCM (6, 7). Interestingly, Echo initially reported the right ventricular (RV) involvement as high risk sign, and deformation and functional abnormality of RV has been related to the increased risk of mortality (8).

Cardiac magnetic resonance

Cardiac magnetic resonance (CMR) imaging provides a necessary information to identify the changes in chamber architecture due to its unsurpassed spatial resolution and ability to directly visualize interstitial abnormalities using gadolinium (Gd) contrast enhancement. Since Maceria et al. initially reported diffuse subendocardial pattern of late gadolinium enhancement, and abnormal T1 shortening compared to hypertensive controls, number of the studies investigated the typical appearance and variation of LGE findings (9). Fontana et al. firstly categorized LGE pattern for CA; no LGE, subendocardial, and diffuse or transmural pattern (10). The several investigators reported high diagnostic accuracy of LGE for CA compared to end-myocardial biopsy as gold standard; sensitivity 86%, specificity 86%, the positive predictive value 95%, and the negative predictive value 67% by Ruberg et al.; sensitivity 80%, specificity 92%, the positive predictive value 92%, and the negative predictive value 85% by Vogelsberg et al. (11, 12). However, characteristic pattern of CMR-LGE for CA can hinder accurate setting of null point due to the nature of diffuse disease. Difficulty of nulling the myocardium itself can strongly suggest CA, but denning CA can be difficult when CMR show no LGE or low contrast signal. A phase sensitive inversion recovery sequence (PSIR) has developed to improve diagnostic performance and reduce operators-dependent null setting (13). Recent CMR analysis using dedicated LGE scoring system (Query Amyloid Late Enhancement) successfully distinguished ATTR CA from AL with high sensitivity (87%) and specificity (96%) compared to histology as referential standard, suggesting noninvasive differentiation of subtype is quite feasible in clinical practice (14). However, CA is a diffuse disease, and has no "normal" myocardium to refer. Quantitative T1 mapping and extracellular volume (ECV) measurement have emerged and shown promising results in diagnosing CA (15). The advantage of quantitative T1 mapping post gadolinium is the measurement of extracellular volume (ECV), which is extracellular matrix expansion due to deposition of amyloid fibrils in myocardium

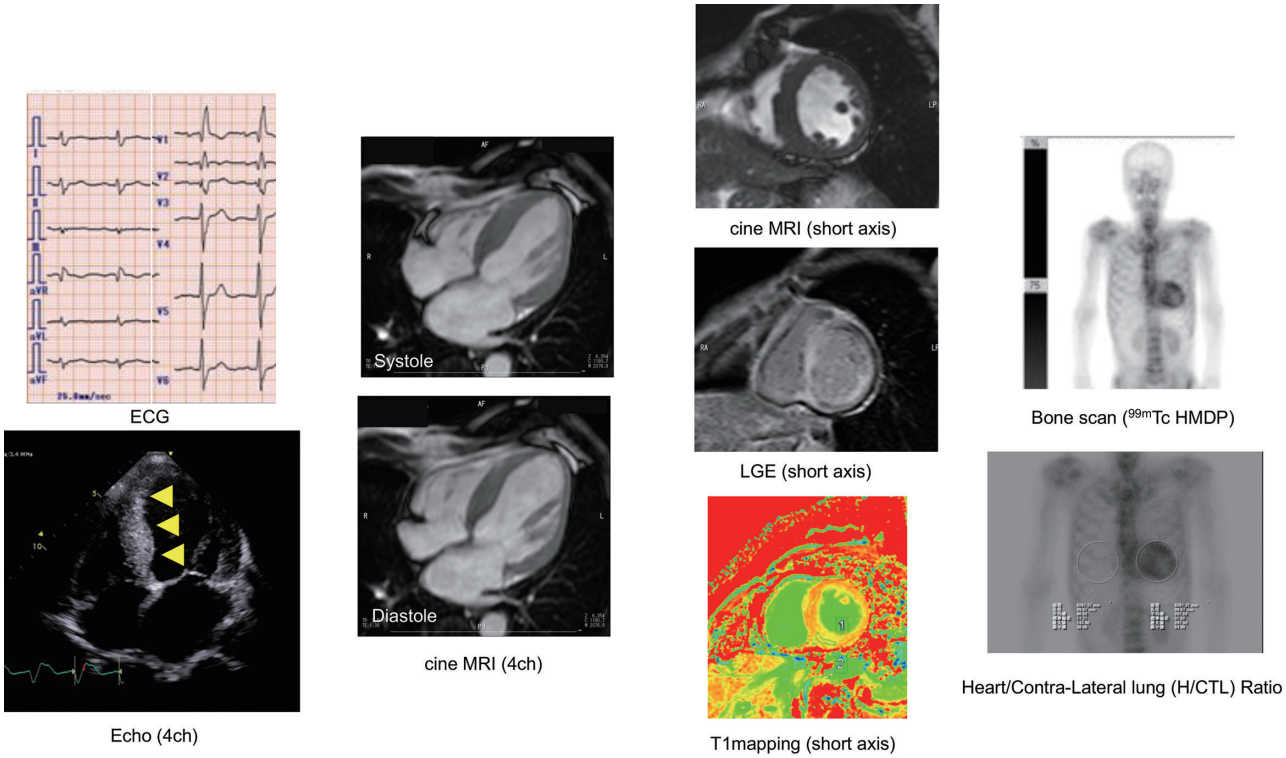

Figure 1

Electrocardiogram and echocardiography of Cardiac Amyloidosis are shown. Relatively low voltage in rim lead in electrocardiogram, which indicate CA (left panel). Right panel shows typical granular sparkling septum in echocardiography (yellow arrows). Cardiac magnetic resonance imaging for Cardiac Amyloidosis is shown. Steady-state free precession cine MRI shows remarkably thickened septal wall with reduced cardiac function and mildly dilated left ventricular is (LVEF is 24.5%, LVEDV index 120mL). Late gadolinium enhancement study shows diffuse hyper intensity of subendocardial to transmural pattern. T1 mapping by modified Look-Locker inversion recovery is shown in the middle. Right upper panel shows whole body planar image of ^{99m}Tc-HMDP bone scan. Remarkable RI uptake in myocardium, and uptake ratio analysis using heart/contra-lateral lung ROI shows 2.51 which strongly indicates ATTR type of cardiac amyloidosis (right lower).

and resulting in the gadolinium contrast penetration. The middle panel of Figure 1 shows representative CMR findings of ATTR type CA. Balanced SSFP cine images for diastole and systole show remarkably thickened septal wall, and reduced global contraction despite preserved LV cavity. Diffuse hyper signal intensity is observed for LGE study, and T1 value can be obtained employing MOLLI sequence (left-middle lower). Recent investigations reported the higher diagnostic performance of LGE combined with T1 mapping post gadolinium compared to conventional assessment (15). However, patients with CA frequently have renal insufficiency, which is the administration of Gd in not adequate due to the increased risk of developing nephrogenic systemic fibrosis. Thus, non-contrast imaging technique is needed. Karamitsos et al. firstly reported the elevation of non-contrast, namely, native T1 mapping in patients with AL CA (16). Moreover, non-contrast, native T1 mapping has a potential to differentiate CA from other hypertrophic cardiomyopathy using optimal cut off value over 1273 ms with high sensitivity (84%) and specificity (89%) (16, 17). Prognostic usefulness of LGE and native or combined with post Gd T1 mapping has been also extensively investigated (10, 18, 19). Additionally, usefulness of native T2 mapping for diagnosing CA has been investigated (20). Several studies have shown the feasibility of new technique over conventional MOLLI sequence to obtain quantitative T1 value (21), but this technique needs to be validated in routine clinical practice. Summarizing above, multiparametric image analysis using PSIR and quantitative measurement using T1 is necessary in diagnosis of CA. The disadvantages of CMR are follows; LGE is not adequate for CKD. Significant generator and lead artifact can occur after device implantation. To date, CMR is rather inadequate for patients with CKD and device implantation, and nuclear imaging is most available imaging including the steps for differentiating subtypes for those patients.

Cardiac PET

In cardiac PET, CA can be visualized using amyloid PET tracers which had been originally designed to detect β amyloid deposition in Alzheimer's disease (22). After the promising results of these compounds in brain imaging, the researchers have emerged into the clinical feasibility of these tracers in

cardiac amyloid deposition. Carbon-11 labaled Pittsburgh compound B (PiB) has been established as derivative of thioflavin-T which had been thoroughly used to bind β amyloid (23). Initial clinical investigation using PiB showed promising results (24). The potential application of PiB PET scans in ATTR and AL amyloid imaging was explored, with promising results. The findings of PiB PET tomography correlated well with post-mortem histopathological samples [68]. Pilebro et al. using PiB for ATTR-CA, showed that type B patients had a higher uptake in myocardium than those with type A (25). Lee et al. reported the reduced PiB retention index in patient with CA after chemotherapy compared to untreated, and this report suggested a potential usefulness of PiB as monitoring tool for therapeutic effect (26). Lee et al. also reported that the cardiac uptake of PiB showed significant predictive value of adverse outcome (27). Rosengren et al., employing quantitative SUV measurement, reported improved diagnostic accuracy of PiB for CA (sensitivity 94%, and specificity 93%) (28).

Fluorine-based tracers have relatively longer half-life and have been widely studied and confirmed a high affinity for cardiac amyloid deposits. Several investigations using ^{18}F Florbetapir which has distinct structure from PiB, reported high affinity for myocardial amyloid deposit in ATTR-CA (29). A study by Park et al. showed strong impact for the specific binding of ^{18}F-Florbetapir proved in an ex vivo analysis using autoradiography (30). This study has also showed a trend for higher myocardial tracer uptake compared to ATTR CA. ^{18}F Flutemetamol is another compound with similar structure. An initial pilot study showed remarkable cardiac uptake in nine subjects out of all ten (31). Another study for ATTR CA with hereditary V30 mutation showed interesting results that the patients with negative uptake for bone scan scintigraphy revealed positive ^{18}F Flutemetamol uptake (32). ^{18}F sodium fluoride (NaF) of which basic physiological property is similar to that of MDP, has been developed as PET tracer for skeletal metastasis and atherosclerosis (33, 34). Although, the evidence has not been well accumulated, advantage of PET tracer to SPECT is well recognized and high resolution with evaluation using SUV values.

^{99m}Tc scintigraphy and SPECTCT

^{99m}Technetium bone avid tracers (Pyrophosphate: PYP, Diphosphono-1,2-propanodicarboxylic acid: DPD, Hydroxymethylene diphosphonate: HMDP, and methylene diphosphonate: MDP) are commonly used for bone scan. These tracers have been extensively utilized in the diagnostic process for CA. Although the exact mechanism of bone seeking tracers binding to the amyloid fibrils remains uncertain, the increased level of microcalcification of the TTR fibrils may be a clue. DPD have demonstrated high diagnostic performance approaching 100% for ATTR CA (35). DPD have demonstrated strong impact in diagnosing of ATTR CA particularly due to clear cut off. A first study reported in 2005, Perugini proposed visual grading for cardiac DPD uptake (Perugini score: grade 1-uptake lower than bone, grade 2-moderate uptake equivalent to bone, grade 3-high uptake stronger than bone), and reported that DPD has relevantly discern ATTR from AL CA (36). However, largest multi-center study yields lower specificity in diagnosing ATTR CA because a low grade uptake was frequently observed in AL CA, while high sensitivity was confirmed (37). Bokhari et al. using PYP for 25 patients, reported that PYP could sufficiently differentiated between ATTR and AL CA (38). The left panel of figure 2 shows a typical and definitive cardiac uptake in whole body bone scan (^{99m}Tc MDP) in patient with ATTR CA, and heart/contra-lateral lung ratio reveals 2.51 which strongly indicates ATTR CA (optimal cut off is 1.5 by Bokhari et al.) (left lower). More recently, bone SPECTCT scan has been widely used to perform quantitative measurement for metastatic bone uptake in oncology field. Figure 2 shows cardiac dual SPECT/CT for PYP and 201TL. Bothe SPECT and polar map PYP image show heterogenous uptake in myocardium (left). Novel SPECTCT using xSPECT system (Simens, Enlargen) enable us to perform quantitative measurement and obtain SUV value (right panel) (39). On the other hand, myocardial bone uptake is not observed in AL CA, while typical diffuse LGE was detected as shown in Figure 3. However, complete differentiation of AL and ATTR using bone seeking tracers seems still insufficient. Other tracers, such as ^{99m}Tc aprotinin, which demonstrated promising potential to detect pre-symptomatic status of CA, and positive findings for AL CA (40). Latest and common relevant technique is to measure cardiac uptake ratio to right lateral lung in planner images (heart to contra-lateral lung ratio＝H/CL ratio), and demonstrated prognostic utility (41, 42).

^{123}I metaiodobenzylguanidine (MIBG) scintigraphy has been also studied in CA. MIBG is capable of visualizing cardiac sympathetic denervation, and has been originally proven its predictive usefulness for lethal arrythmia, heart failure, or death for ischemic and nonischemic cardiomyopathy. Although MIBG is not suitable for diagnosis of CA, has a potential of evaluating the increased risk of future cardiac event and therapeutic effect (43, 44).

Future direction

As widely recognized, the treatment options vary for the different types of CA including chemotherapy established in decades ago. Tafamidis (Vyndaqel®) is a tetramer stabilizer which prevents amyloidgenesis, formerly approved for preventive treatment of FAP. Randomized control trial

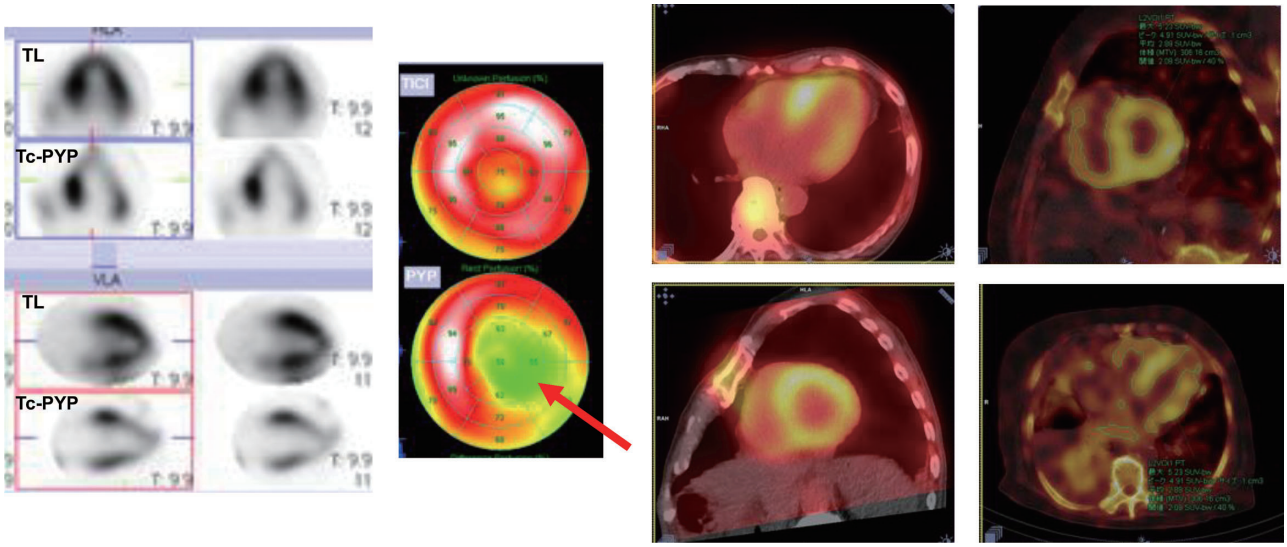

Figure 2
Dual isotope imaging using 201TL, and ^{99m}Tc pyrophosphate (PYP) SPECT for cardiac amyloidosis is shown. PYP image shows heterogenous uptake while TL-SPECT imaging shows almost normal perfusion. Using dedicated software (Syngo via, with xSPECT system), myocardial uptake can be quantitatively assessed.

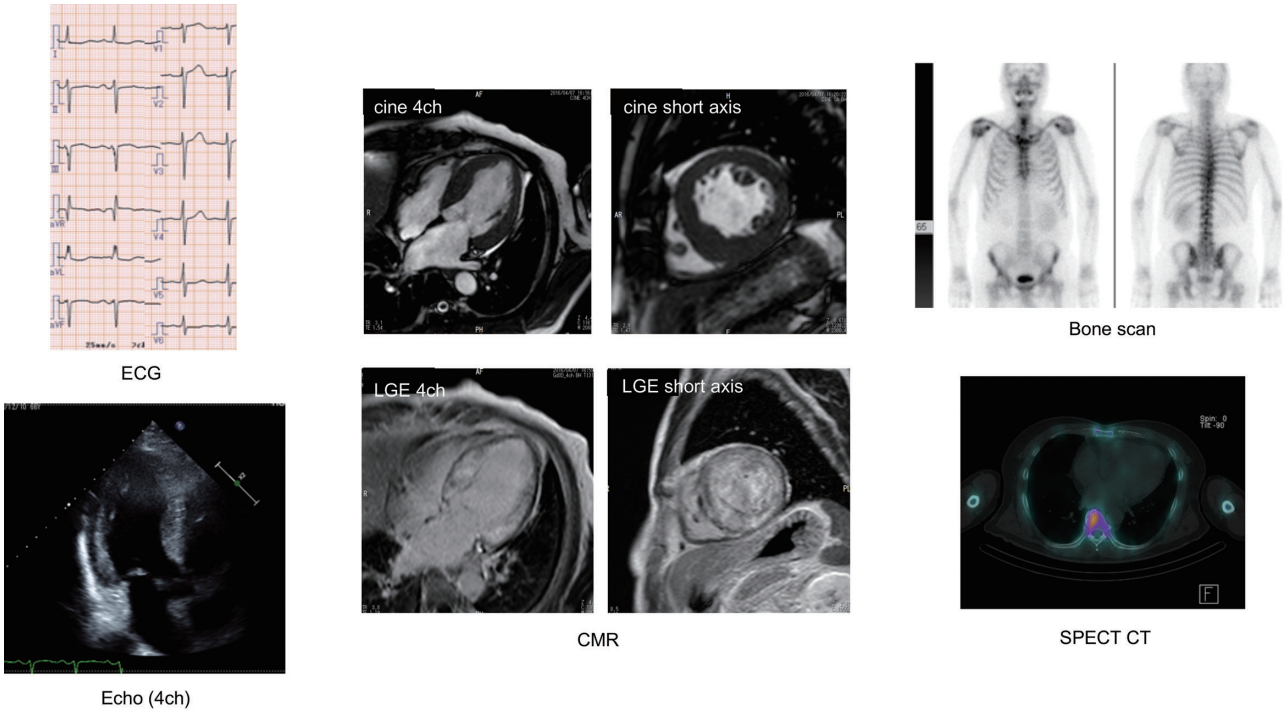

Figure 3
Representative case of biopsy-proven AL type cardiac amyloidosis is shown. Cine MRI shows significant left ventricular hypertrophy with suspect of asymmetric septal hypertrophy (middle panel). Late gadolinium enhancement shows diffuse hyper intensity, while no uptake observed for ^{99m}Tc HMDP scintigraphy (right upper) and SPECT/CT (right lower), which indicated the compatibility for AL type, and less possibility for ATTR.

compared to placebo succeeded to prove the efficacy of Tafamidis in patients with ATTR CA (45). Temporary, other treatment options are entering the market or under investigation. The role of noninvasive imaging should move towards different level beyond conventional diagnosis to prediction and monitoring therapeutic effect.

Reprint requests and correspondence:
Kenji Fukushima, MD, PhD
Department of Nuclear Medicine, Heart Center, Saitama Medical University International Medical Center, 1397-1 Yamane, Hidaka, Saitama, 350-1298, Japan
E-mail: kfukush4@saitama-med.ac.jp

References

1. Bhogal S, Ladia V, Sitwala P, Cook E, Bajaj K, Ramu V, et al. Cardiac amyloidosis: an updated review with emphasis on diagnosis and future directions. Curr Probl Cardiol 2018; 43: 10–34.
2. Martinez-Naharro A, Baksi AJ, Hawkins PN, Fontana M. Diagnostic imaging of cardiac amyloidosis. Nat Rev Cardiol 2020; 17: 413–26.
3. Oerlemans MIFJ, Rutten KHG, Minnema MC, Raymakers RAP, Asselbergs FW, de Jonge N. Cardiac amyloidosis: the need for early diagnosis. Neth Heart J 2019; 27: 525–36.
4. Cacciapuoti F. The role of echocardiography in the non-invasive diagnosis of cardiac amyloidosis. J Echocardiogr 2015; 13: 84–9.
5. Di Bella G, Pizzino F, Minutoli F, Zito C, Donato R, Dattilo G, et al. The mosaic of the cardiac amyloidosis diagnosis: role of imaging in subtypes and stages of the disease. Eur Heart J Cardiovasc Imaging 2014; 15: 1307–15.
6. Pagourelias ED, Mirea O, Duchenne J, Van Cleemput J, Delforge M, Bogaert J, et al. Echo parameters for differential diagnosis in cardiac amyloidosis: a head-to-head comparison of deformation and nondeformation parameters. Circ Cardiovasc Imaging 2017; 10: e005588.
7. Baccouche H, Maunz M, Beck T, Gaa E, Banzhaf M, Knayer U, et al. Differentiating cardiac amyloidosis and hypertrophic cardiomyopathy by use of three-dimensional speckle tracking echocardiography. Echocardiography 2012; 29: 668–77.
8. Siddiqi OK, Sanchorawala V, Ruberg FL. Echocardiography and survival in light chain cardiac amyloidosis: back to basics. Circ Cardiovasc Imaging 2018; 11: e007826.
9. Maceira AM, Joshi J, Prasad SK, Moon JC, Perugini E, Harding I, et al. Cardiovascular magnetic resonance in cardiac amyloidosis. Circulation 2005; 111: 186–93.
10. Fontana M, Pica S, Reant P, Abdel-Gadir A, Treibel TA, Banypersad SM, et al. Prognostic value of late gadolinium enhancement cardiovascular magnetic resonance in cardiac amyloidosis. Circulation 2015; 132: 1570–9.
11. Ruberg FL, Appelbaum E, Davidoff R, Ozonoff A, Kissinger KV, Harrigan C, et al. Diagnostic and prognostic utility of cardiovascular magnetic resonance imaging in light-chain cardiac amyloidosis. Am J Cardiol 2009; 103: 544–9.
12. Vogelsberg H, Mahrholdt H, Deluigi CC, Yilmaz A, Kispert EM, Greulich S, et al. Cardiovascular magnetic resonance in clinically suspected cardiac amyloidosis: noninvasive imaging compared to endomyocardial biopsy. J Am Coll Cardiol 2008; 51: 1022–30.
13. Syed IS, Glockner JF, Feng D, Araoz PA, Martinez MW, Edwards WD, et al. Role of cardiac magnetic resonance imaging in the detection of cardiac amyloidosis. JACC Cardiovasc Imaging 2010; 3: 155–64.
14. Dungu JN, Valencia O, Pinney JH, Gibbs SD, Rowczenio D, Gilbertson JA, et al. CMR-based differentiation of AL and ATTR cardiac amyloidosis. JACC Cardiovasc Imaging 2014; 7: 133–42.
15. Mongeon FP, Jerosch-Herold M, Coelho-Filho OR, Blankstein R, Falk RH, Kwong RY. Quantification of extracellular matrix expansion by CMR in infiltrative heart disease. JACC Cardiovasc Imaging 2012; 5: 897–907.
16. Karamitsos TD, Piechnik SK, Banypersad SM, Fontana M, Ntusi NB, Ferreira VM, et al. Noncontrast T1 mapping for the diagnosis of cardiac amyloidosis. JACC Cardiovasc Imaging 2013; 6: 488–97.
17. Fontana M, Banypersad SM, Treibel TA, Maestrini V, Sado DM, White SK, et al. Native T1 mapping in transthyretin amyloidosis. JACC Cardiovasc Imaging 2014; 7: 157–65.
18. Maurer M, Castaño A. Prognosticating in cardiac amyloidosis: let me count the ways. JACC Cardiovasc Imaging 2019; 12: 834–6.
19. Austin BA, Tang WHW, Rodriguez ER, Tan C, Flamm SD, Taylor DO, et al. Delayed hyper-enhancement magnetic resonance imaging provides incremental diagnostic and prognostic utility in suspected cardiac amyloidosis. JACC Cardiovasc Imaging 2009; 2: 1369–77.
20. Ridouani F, Damy T, Tacher V, Derbel H, Legou F, Sifaoui I, et al. Myocardial native T2 measurement to differentiate light-chain and transthyretin cardiac amyloidosis and assess prognosis. J Cardiovasc Magn Reson 2018; 20: 58.
21. Shao J, Rashid S, Renella P, Nguyen KL, Hu P. Myocardial T1 mapping for patients with implanted cardiac devices using wideband inversion recovery spoiled gradient echo readout. Magn Reson Med 2017; 77: 1495–504.
22. Small GW, Kepe V, Ercoli LM, Siddarth P, Bookheimer SY, Miller KJ, et al. PET of brain amyloid and tau in mild cognitive impairment. N Engl J Med 2006; 355: 2652–63.
23. Nordberg A, Carter SF, Rinne J, Drzezga A, Brooks DJ, Vandenberghe R, et al. A European multicentre PET study of fibrillar amyloid in Alzheimer's disease. Eur J Nucl Med Mol Imaging 2013; 40: 104–14.
24. Antoni G, Lubberink M, Estrada S, Axelsson J, Carlson K, Lindsjö L, et al. In vivo visualization of amyloid deposits in the heart with ^{11}C-PIB and PET. J Nucl Med 2013; 54: 213–20.
25. Pilebro B, Arvidsson S, Lindqvist P, Sundström T, Westermark P, Antoni G, et al. Positron emission tomography (PET) utilizing Pittsburgh compound B (PIB) for detection of amyloid heart deposits in hereditary transthyretin amyloidosis (ATTR). J Nucl Cardiol 2018; 25: 240–8.
26. Lee SP, Lee ES, Choi H, Im HJ, Koh Y, Lee MH, et al. ^{11}C-Pittsburgh B PET imaging in cardiac amyloidosis. JACC Cardiovasc Imaging 2015; 8: 50–9.
27. Lee SP, Suh HY, Park S, Oh S, Kwak SG, Kim HM, et al. Pittsburgh B compound positron emission tomography in patients with AL cardiac amyloidosis. J Am Coll Cardiol 2020; 75: 380–90.
28. Rosengren S, Skibsted Clemmensen T, Tolbod L, Granstam SO, Eiskjaer H, Wikström G, et al. Diagnostic accuracy of [^{11}C] PIB positron emission tomography for detection of cardiac amyloidosis. JACC Cardiovasc Imaging 2020; 13: 1337–47.
29. Dorbala S, Vangala D, Semer J, Strader C, Bruyere JR Jr., Di Carli MF, et al. Imaging cardiac amyloidosis: a pilot study using (1) (8)F-florbetapir positron emission tomography. Eur J Nucl Med Mol Imaging 2014; 41: 1652–62.
30. Park MA, Padera RF, Belanger A, Dubey S, Hwang DH, Veeranna V, et al. ^{18}F-florbetapir binds specifically to myocardial light chain and transthyretin amyloid deposits: autoradiography study. Circ Cardiovasc Imaging 2015; 8.

31. Dietemann S, Nkoulou R. Amyloid PET imaging in cardiac amyloidosis: a pilot study using 18F-flutemetamol positron emission tomography. Ann Nucl Med 2019; 33: 624–8.
32. Möckelind S, Axelsson J, Pilebro B, Lindqvist P, Suhr OB, Sundström T. Quantification of cardiac amyloid with [^{18}F] Flutemetamol in patients with V30M hereditary transthyretin amyloidosis. Amyloid 2020; 27: 191–9.
33. Høilund-Carlsen PF, Sturek M, Alavi A, Gerke O. Atherosclerosis imaging with ^{18}F-sodium fluoride PET: state-of-the-art review. Eur J Nucl Med Mol Imaging 2020; 47: 1538–51.
34. McKenney-Drake ML, Moghbel MC, Paydary K, Alloosh M, Houshmand S, Moe S, et al. ^{18}F-NaF and ^{18}F-FDG as molecular probes in the evaluation of atherosclerosis. Eur J Nucl Med Mol Imaging 2018; 45: 2190–200.
35. Rapezzi C, Quarta CC, Guidalotti PL, Pettinato C, Fanti S, Leone O, et al. Role of ^{99m}Tc-DPD scintigraphy in diagnosis and prognosis of hereditary transthyretin-related cardiac amyloidosis. JACC Cardiovasc Imaging 2011; 4: 659–70.
36. Perugini E, Guidalotti PL, Salvi F, Cooke RMT, Pettinato C, Riva L, et al. (2005) Noninvasive etiologic diagnosis of cardiac amyloidosis using ^{99m}Tc-3, 3-diphosphono-1, 2-propanodicarboxylic acid scintigraphy. J Am Coll Cardiol 2005; 46: 1076–84.
37. Gillmore JD, Maurer MS, Falk RH, Merlini G, Damy T, Dispenzieri A, Wechalekar AD, et al. Nonbiopsy diagnosis of cardiac transthyretin amyloidosis. Circulation 2016; 133: 2404–12.
38. Bokhari S, Castaño A, Pozniakoff T, Deslisle S, Latif F, Maurer MS. ^{99m}Tc-pyrophosphate scintigraphy for differentiating light-chain cardiac amyloidosis from the transthyretin-related familial and senile cardiac amyloidoses. Circ Cardiovasc Imaging 2013; 6: 195–201.
39. Caobelli F, Braun M, Haaf P, Wild D, Zellweger MJ. Quantitative ^{99m}Tc-DPD SPECT/CT in patients with suspected ATTR cardiac amyloidosis: Feasibility and correlation with visual scores. J Nucl Cardiol 2019. [Online ahead of print]
40. Awaya T, Minamimoto R, Iwama K, Kubota S, Hotta M, Hirai R, et al. Performance of ^{99m}Tc-aprotinin scintigraphy for diagnosing light chain (AL) cardiac amyloidosis confirmed by endomyocardial biopsy. J Nucl Cardiol 2019. [Online ahead of print]
41. Castano A, Haq M, Narotsky DL, Goldsmith J, Weinberg RL, Morgenstern R, et al. Multicenter study of planar technetium 99m pyrophosphate cardiac imaging: predicting survival for patients with ATTR cardiac amyloidosis. JAMA Cardiol 2016; 1: 880–9.
42. Sperry BW, Vranian MN, Tower-Rader A, Hachamovitch R, Hanna M, Brunken R, et al. Regional variation in technetium pyrophosphate uptake in transthyretin cardiac amyloidosis and impact on mortality. JACC Cardiovasc Imaging 2018; 11: 234–42.
43. Piekarski E, Chequer R, Algalarrondo V, Eliahou L, Mahida B, Vigne J, et al. Cardiac denervation evidenced by MIBG occurs earlier than amyloid deposits detection by diphosphonate scintigraphy in TTR mutation carriers. Eur J Nucl Med Mol Imaging 2018; 45: 1108–18.
44. Slart RHJA, Glaudemans AWJM, Hazenberg BPC, Noordzij W. Imaging cardiac innervation in amyloidosis. J Nucl Cardiol 2019; 26: 174–87.
45. Maurer MS, Schwartz JH, Gundapaneni B, Elliott PM, Merlini G, Waddington-Cruz M, et al. Tafamidis treatment for patients with transthyretin amyloid cardiomyopathy. N Engl J Med 2018; 379: 1007–16.